

# Strong asymmetry of forward scattering effect from dielectric nanoantenna in media

Pavel D. Terekhov,<sup>†‡¶§</sup> Hadi K. Shamkhi,<sup>‡</sup> Egor Gurvitz,<sup>‡</sup> Andrey B. Evlyukhin,<sup>||</sup> Alexander S. Shalin,<sup>‡</sup> Alina Karabchevsky<sup>†¶§</sup>

*†Electrooptics and Photonics Engineering Department, Ben-Gurion University, Beer-Sheva  
8410501, Israel*

*‡ ITMO University, 49 Kronverksky Ave., 197101, St. Petersburg, Russia*

*¶ Ilse Katz Institute for Nanoscale Science & Technology, Ben-Gurion University, Beer-Sheva  
8410501, Israel*

*§ Center for Quantum Information Science and Technology, Ben-Gurion University, Beer-Sheva  
8410501, Israel*

*|| Centre for Nano Optics, University of Southern Denmark, Campusvej 55, DK-5230, Odense M,  
Denmark*

## Abstract

Dielectric photonics platforms provide unique possibilities to control the light scattering effect of high-index dielectric particles. Despite the intensively growing field of all-dielectric nanophotonics, it is still unclear how the media influence on scattering properties of a particle. Here we report on the scattering effect of a silicon nanoantenna embedded in media. We show that the higher the index of media is, the less confined field appears in the dielectric nanoantenna; in addition, the induced electro-magnetic multipole resonances endorse different red-shifts and broadening over the whole visible spectrum. For a comprehensive analysis, we introduce the asymmetry parameter of the Cartesian multipole moments and show that the overlapping of the broadened multipoles leads to the strong forward directivity. We notice that dielectric nanoantenna embedded in a high-index media supports broadband forward light scattering and amplification. Outcomes of our research are essential for the applications such as sensing and healthcare in which the influence of the media is crucial.

## Introduction

Tuning the scattering resonances of plasmonic or dielectric nanoparticles has enabled scientists and engineers to localize light and enhance peculiar optical phenomena over the last decade<sup>1,2</sup>. Specifically, by changing the shape and dimensions of high-index dielectric nanoparticles, their optical properties change, leading to the interesting phenomena<sup>2-7</sup>. Nanoparticles scatter the light and support the excitation of the geometrical (Mie) electric and magnetic multipolar resonance<sup>2-8</sup> which in turn enhance the light-matter interaction. Even if the influence of nanoparticles size, geometry, and material on their optical properties have been extensively explored<sup>3,9,10</sup>, the influence of media in which nanoparticles are embedded is still puzzling. Here, therefore, we address this knowledge gap by exploring the optical properties of the high-index nanocubes depending on the optical properties of media. Despite the large scattering cross-section when confining the currents<sup>11</sup>, all-dielectric nanoparticles, compared to plasmonic<sup>1,12,13</sup>, do not exhibit Joule losses<sup>14</sup>. One of the suitable methods of understanding interactions of light with nanoparticles, the multipole decomposition<sup>15</sup>, is usually geared towards isolated specks of matter suspended in vacuum. Here, for the first time, we systematically study the scattering effect by the high-index nanoparticles due to the tuning of the optical properties of a medium.

The possibility to control light using the appropriate multipole contributions to the scattering process can be used for different applications, including nanoantennas<sup>16-20</sup>, sensors<sup>21-23</sup>, solar cells<sup>24</sup>, multi-functional metasurfaces<sup>25,26</sup> and cloaks<sup>13,27</sup>. Dielectric nanoparticles could be used for a drug delivery and as probes for an electromagnetic diagnosis in emerging medical applications<sup>28-30</sup>. The particles' behavior in the dielectric media like, roughly, the human body environment is the other very interesting question<sup>31</sup>. Here, we use the multipole decomposition approach<sup>32,33</sup>, successfully

implemented previously to study the single particles in air in the optical<sup>3,14</sup> and terahertz<sup>8,34</sup> spectral ranges.

Here, for the first time, we numerically study the multipole spectral evolution in the single silicon nanocubes while tuning the refractive index of surrounding media. We analyse the spectral positions and the absolute contributions of multipoles to the scattering cross-section and compare their collective response in different media. Hereupon, we notice the intriguing effect of broadband forward scattering in high-index media. Insights from this study are expected to pave the way toward engineering the nanophotonic systems in media within a single frame-work.

## Theoretical Background

In this paper, we consider the optical system including the single nanocube suspended in a medium. As shown in Fig.1, We study a nanocube with the edge of  $H = 250 \text{ nm}$ , made of polycrystalline silicon<sup>35</sup> and suspended in a media with the indexes of  $1 \leq n \leq 2$  with the refractive index increment of  $dn = 0.2$ . Note that the wavelengths values throughout the article are considered for the incident light wave in air.

To analyze the considered system we use the semi-analytical multipole decomposition approach presented in Refs. <sup>32,33</sup>. We use the expressions of the dynamic multipole moments (up to the magnetic quadrupole) as defined in Ref.<sup>33</sup> In addition, we consider the quasistatic electric octupole moment as derived in Ref <sup>32</sup>. The considered set of multipole moments is sufficient for the proper description of the considered system. To obtain the multipole moments excited in the system we use the finite elements method (FEM) implemented in the COMSOL Multiphysics commercial package<sup>36</sup>.

## Asymmetry parameter

The asymmetry parameter is the efficiency factor that quantifies the directivity of light scattering. To derive and calculate the asymmetry parameter for an arbitrarily shaped particle, we apply the Cartesian multipole decomposition method described above for the scattered field. Then, the scattered electric field  $\mathbf{E}_{sca}$  by a particle in homogenous host medium is the superposition of the induced multipole moments contributions:<sup>32</sup>

$$\begin{aligned} \mathbf{E}_{sca}(\mathbf{r}) \cong & \frac{e^{ik_d r}}{r} \frac{k_0^2}{4\pi\epsilon_0} \left( [\mathbf{n} \times [\mathbf{D} \times \mathbf{n}]] + \frac{1}{v_d} [\mathbf{m} \times \mathbf{n}] + \frac{ik_d}{6} [\mathbf{n} \times [\mathbf{n} \times (\hat{Q} \cdot \mathbf{n})]] \right) \\ & + \frac{ik_d}{2v_d} [\mathbf{n} \times (\hat{M} \cdot \mathbf{n})] + \frac{k_d^2}{6} [\mathbf{n} \times [\mathbf{n} \times (\hat{O} \cdot \mathbf{n} \cdot \mathbf{n})]] \end{aligned} \quad (1)$$

where the unit vector  $\mathbf{n}$  is in the direction of scattering vector  $\mathbf{r}$ ,  $\epsilon_d$  is the relative dielectric permittivity of the surrounding medium,  $\epsilon_0$  and  $\mu_0$  are the vacuum electric permittivity and magnetic permeability,  $v_d = c/\sqrt{\epsilon_d}$  is the light speed in the surrounding medium and  $c$  is the light speed in the vacuum;  $k_0$  and  $k_d$  are the wavenumbers in vacuum and in the surrounding medium, respectively.  $\mathbf{m}$  is the magnetic dipole moment (MD);  $\mathbf{D}$  is the total electric dipole moment (TED);  $\hat{Q}$ ,  $\hat{M}$  and  $\hat{O}$  are the electric quadrupole moment tensor (EQ), the magnetic quadrupole moment tensor (MQ) and the tensor of electric octupole moment (OCT), respectively. Note that these tensors are symmetric and traceless and in tensor notation e.g.  $\hat{Q}$  is equal to  $Q_{\alpha\beta}$ , where subscript indices denote components (e.g.  $\alpha = \{x, y, z\}$ )<sup>32</sup>. The scattering cross-section can be presented as (see<sup>32</sup> for details):

$$\begin{aligned} C_{sca} \cong & \frac{k_0^4}{6\pi\epsilon_0^2 |\mathbf{E}_{inc}|^2} |\mathbf{D}|^2 + \frac{k_0^4 \epsilon_d \mu_0}{6\pi\epsilon_0 |\mathbf{E}_{inc}|^2} |\mathbf{m}|^2 + \frac{k_0^6 \epsilon_d}{720\pi\epsilon_0^2 |\mathbf{E}_{inc}|^2} |\hat{Q}|^2 \\ & + \frac{k_0^6 \epsilon_d^2}{80\pi\epsilon_0 |\mathbf{E}_{inc}|^2} |\hat{M}|^2 + \frac{k_0^8 \epsilon_d^2}{1890\pi\epsilon_0^2 |\mathbf{E}_{inc}|^2} |\hat{O}|^2, \end{aligned} \quad (2)$$

where  $\mathbf{E}_{\text{inc}}$  is the electric field amplitude of the incident light wave. The total scattering cross-section is obtained through the integration of the Pointing vector over a closed surface in the far-field zone and the normalization to the incident field intensity<sup>32</sup>. The asymmetry parameter is the ratio of the cosine-weighted scattering cross section over the total scattering cross section  $C_{\text{sca}}$  and can be calculated as

$$g = \frac{1}{|\mathbf{E}_{\text{inc}}|^2 C_{\text{sca}}} \int |\mathbf{E}_{\text{sca}}|^2 r^2 \cos \theta d\Omega \quad (3)$$

after the integrating over the solid angle  $d\Omega = \sin \theta d\theta d\phi$ , we find

$$g \cong \frac{1}{|\mathbf{E}_{\text{inc}}|^2 C_{\text{sca}}} \frac{k_0^4}{360\pi\epsilon_0^2 v_d^2} \left[ 60v_d \Re\{D_x m_y^* - D_y^* m_x\} - 6k_d v_d^2 \Im\{D_\alpha Q_{\alpha z}^*\} \right. \\ \left. - 18k_d \Im\{m_\alpha M_{\alpha z}^*\} - k_d^2 v_d \Re\{Q_{y\alpha}^* M_{x\alpha} - Q_{x\alpha}^* M_{y\alpha}\} \right. \\ \left. - \frac{24}{315} k_d^3 v_d^2 \Im\{Q_{\beta\beta} O_{\alpha\alpha z}^* + 2Q_{\beta z} O_{\beta\alpha\alpha}^* - 5Q_{\alpha\beta} O_{\alpha\beta z}^*\} \right]. \quad (4)$$

Physically,  $I_{\text{inc}}(1 - g)C_{\text{sca}}$  is the net rate of momentum transferring to the particle in the direction of the propagation where  $I_{\text{inc}}$  is the irradiance of the incident light beam. Upon inspection of the asymmetry parameter formula presented above, all multipoles interplays terms that scatter the light symmetrically along the scattering polar angle  $\theta = 90^\circ$  have vanished; that includes the electromagnetic multipoles coherence from different orders. Therefore, the asymmetry parameter is a measure of light directivity; meaning that, its zero value corresponds to equal distribution of the power scattered in both half spaces. Its evolution to the lower half space (forward) and the upper half space (backward) results in positive and negative values, respectively. Furthermore, important and well-known Kerker effect for dipoles and Kerker-like effects for high-order multipoles can be understood with the asymmetry parameter equations. If we consider the case of  $E_x$  polarized incident light, then Kerker condition of ED and MD fulfills when the ratio  $v_d D_x / m_y = 1$  with  $g = 0.5$ . Kerker-

like condition of TED and EQ interplay fulfills at  $6iD_x/k_d Q_{xz} = 1$  while for the MD and MQ interplay it fulfills when  $2im_y/k_d M_{yz} = 1$ . Consequently, the EQ and MQ interplay scatter in forward directions when  $v_d Q_{xz}/3M_{yz} = 1$  and finally for EQ and EO coherence the condition is  $5Q_{xz}/4ik_d O_{zzx} = 1$ . Generally, the synchronous multipole couplings enhance the field directionality, and play a key role for the suppression of the backscattering.

Total electric fields and the corresponding induced polarization in the scatterers are calculated numerically using COMSOL Multiphysics. Using the calculated polarization, the multipole moments and their contributions into scattering cross-sections and the asymmetry parameter are obtained by a numerical integration.

In the next section we analyze in details the results obtained for the different surrounding media and the multipoles behavior in the system.

## **Results and discussion**

### **Multipole decomposition spectra evolution**

To analyze the optical properties of the considered nanoparticle in different media, we draw the multipole decomposition of the scattering cross-section spectra for the six different cases of  $1 \leq n \leq 2$  (Fig. 2). To prove that our multipole decomposition approach can be applied, we compare the scattering cross-section as the sum of multipole contributions (Sum Scat) and the scattering cross-section obtained with the direct calculation (Total scat (COMSOL)) for every case. As discussed in the Supplementary material, this comparison shows the good coincidence between the calculation methods when we use the dynamic multipole moments.

We start our analysis with the case of the particle embedded in air. The case of  $n = 1$  (Fig. 2a) has been considered in detail in<sup>3</sup> for the similar nanoantenna. One can note the pronounced resonant peaks in the scattering cross-section spectrum; as can be noted from Fig. 2, these peaks are associated with the resonant excitations of the total electric dipole (TED) moment, the magnetic dipole (MD) moment, the electric quadrupole (EQ) moment and the magnetic quadrupole (MQ) moment. In this work, we explore the behavior of these multipole resonances as we increase  $n$  up to  $n = 2$ . Fig. 2b shows that starting from  $n = 1.2$  the scattering cross-section resonant peaks start to merge with each other. At  $\lambda = 640 \text{ nm}$ , the scattering cross-section peak is now due to the interaction between MD and EQ moments forming the one wider scattering peak. Similarly, the EQ and MQ moments resonant peaks begin to merge into the single peak around  $\lambda = 750 \text{ nm}$ , but for  $n = 1.2$  they still can be distinguished. At last, the TED and MD resonances in the near-infrared spectral range experience some broadening and become a bit smoother. However, the spectra for  $n = 1.2$  is still close to the case of air medium.

For  $n = 1.4$  (Fig. 2c), the MQ and EQ resonant peaks merge to the single scattering cross-section peak at  $\lambda = 790 \text{ nm}$ . At the same time, the TED and MD resonances in the near-infrared spectral range continue their broadening; the TED resonant excitation no longer leads to the separate scattering cross-section peak. Finally, the EQ and MQ resonances continue to merge and provide the scattering cross-section peak together at  $\lambda = 650 \text{ nm}$ . In the case of  $n = 1.4$  only three scattering peaks can be distinguished.

Next, we consider  $n = 1.6$  which is approximately equal to the refractive index of immersion oils (Fig. 2d). The EQ moment still experiences the bigger red shift in comparison with the magnetic multipole moments MQ and MD. For  $n = 1.6$ , one can note the resonant excitation of electric octupole moment (OCT) at  $\lambda = 620 \text{ nm}$ . We also expect the excitation of multipole moments of

higher orders in this wavelength region, but the moments taken into account are enough for a proper description of the system. It is worth noting that OCT contributes to the scattering peak formed by EQ and MD at  $\lambda = 650 \text{ nm}$ . At the region of longer wavelengths, the spectral position of MQ and EQ resonances match each other at  $\lambda = 795 \text{ nm}$  and the resulting scattering cross-section peak is well pronounced in Fig. 2d. The MD-induced scattering cross-section peak can be still noted at  $\lambda = 1160 \text{ nm}$ . Such intermediate case still shows the three scattering cross-section peaks, but some broadening can be noted.

The final stage of our multipole decomposition study is presented in Fig. 2e,f for  $n = 1.8$  and  $n = 2$ . In the wavelength range  $600 \leq \lambda \leq 700 \text{ nm}$ , the resonant excitation of OCT provides the incremental contribution to the scattering cross-section. This contribution, together with the EQ and MD resonant excitations and the non-resonant MQ contribution, forms the scattering cross-section peak at the considered region. The EQ moment resonance continues its shifting to the red zone with respect to the MQ resonant area; hence, their joint scattering cross-section peak becomes smoother ( $\lambda = 810 \text{ nm}$ ). The MD-induced scattering peak at  $\lambda \approx 1170 \text{ nm}$  is almost smoothed out for  $n = 2$ .

To provide the better visibility of the multipole evolution in Fig. 3, we show the evolution of each multipole as  $n$  changes. The evolution of dipole moments is shown in Fig. 3a,b for the TED and MD correspondingly; the evolution of the quadrupole moments is shown in Fig. 3c,d for the EQ and MQ correspondingly. Fig. 3a clearly shows that the TED resonant area becomes broader, but the peak value decreases as  $n$  rises. Moreover, the TED resonant region experiences a relatively strong redshift as  $n$  rises. Similarly, the MD resonance at  $\lambda \approx 1150 \text{ nm}$  (Fig. 3b) experiences broadening, but the maximum contribution decreases as  $n$  rises. However, for the second MD resonance at  $\lambda \approx 660 \text{ nm}$ , the maximum contribution can be noted for  $n = 1.4$ . Some broadening can be also noticed for the second resonance. In addition, both resonant areas experience the little redshift.

Interestingly, the quadrupole resonances (Fig. 3c,d) behave slightly differently. As shown in Fig3c, both EQ resonances experience the redshift; it is especially strong for the resonant excitation at longer wavelengths, where the EQ resonant peak shifts from  $\lambda = 700 \text{ nm}$  for  $n = 1$  to  $\lambda = 880 \text{ nm}$  for  $n = 2$ . The maximum value of contribution to the scattering cross-section for this resonance increases as  $n$  rises. For the resonance in the wavelength region  $600 \text{ nm} \leq \lambda \leq 700 \text{ nm}$ , this parameter reaches its maximum for  $n = 1.8$ . Both EQ resonant regions experience some broadening; we can also note that the overall contribution of the EQ moment to the scattering cross-section increases as  $n$  rises. Further, the MQ moment has the only one resonant area for the considered system (Fig. 3d). This resonance experiences the noticeable redshift, but it is weak in comparison with the redshift of the EQ moment. The MQ resonance shows the broadening as  $n$  rises, but the maximum value of the MQ contribution decreases until  $n$  reaches 1.6 and then rises. Thus, we can associate the behavior of certain multipole moments with the changing of the refractive index of the media.

Such comparative analysis allows the study of the evolution of each multipole contribution to the scattering cross-section and to compare their behavior with each other. For example, we prove that electric multipole resonances experience a stronger redshift than their magnetic counterparts as  $n$  increases. In addition, we show that the dipole moments contributions weaken, while the quadrupole moments contributions, in general, get stronger with  $n$ . These insights can be used to design specific combinations of the multipole moments for tuning the direction of the light scattering.

We can note that the spectral contributions of multipole moments significantly change with  $n$ . Excluding the dipoles-induced scattering cross-section peak in the red part of the spectrum, the overall scattering increases. In addition, the separated peaks merge, hence, the scattering peaks for higher  $n$  smooth out and broaden. Such evolution strongly affects the far-field scattering of the

considered nanoantenna and the electric field distribution inside it. A more detailed consideration can be found in the next section.

## **Far-field scattering and electric field distribution inside the particle**

For a closer analysis of the multipole evolution influence to the optical properties of the system, we first consider the far-field scattering diagrams. For a proper comparison, we consider the wavelength of the MQ resonance for every  $n$  taken into account (Fig. 4).

Separate MQ resonance appearing for  $n = 1$ , provides the MQ - associated radiation pattern with 4 lobes (Fig. 4a); in this case, the side-scattering lobes are directed along the magnetic field polarization of the incident wave<sup>3</sup>. Starting with  $n = 1.2$ , this peculiar radiation pattern reshapes due to the EQ resonant contribution shifting to the MQ resonant area. In Fig. 4b, one can see that the backscattering suppresses due to the destructive interference with the EQ contribution, but the forward scattering rises due to the constructive interference in the forward direction; some homogeneous side-scattering appears due to the influence of the side lobes associated with both EQ and MQ moments. This effect becomes stronger for  $n = 1.4$  (Fig. 4c) and  $n = 1.6$  (Fig. 4d), when the EQ and MQ resonances merge and form the joint scattering cross-section peak (see Fig. 2c,d). In addition, the forward scattering increases in comparison with the case of  $n = 1.2$ . However, some side-scattering still can be noticed and associated with the EQ and MQ contributions.

Fig 4e,f presents the far-field scattering diagrams for  $n = 1.8$  and  $n = 2$  correspondingly. For these cases, the additional contributions of the dipole moments (TED and MD) take place (see Fig. 2e,f). These contributions explain the suppression of the side scattering lobes: due to the mutual interaction between all four multipole moments, the radiation pattern in Fig. 4f represents a very sharp and pronounced forward scattering in presence of the small side-scattering lobes. Thus, such particles can be used as highly directive nanoantennas in high-refractive index media.

To reinforce our investigation, in Fig. 5 we consider the electric field distribution inside the particle for the three different cases. We choose  $n = 1$ ,  $n = 1.6$  and  $n = 2$  for the comparison. The considered wavelengths are similar to those presented in Fig. 4a,d,f and correspond to the MQ resonant wavelength for each case. In Fig. 5a, one can note the electric field distribution which corresponds to the case of the separate magnetic quadrupole; the electric field concentrated almost the same in the front and back sides of the nanoantenna as well as in the side parts, corresponding to the direction of the magnetic field polarization of the incident wave. Fig. 5b shows that for  $n = 1.6$ , the electric field concentrated mostly in the front part of the nanoantenna, despite some weaker concentration in the back and side parts. This distribution corresponds to the far-field radiation pattern presented in Fig. 4d. Finally, in Fig. 5c, almost all of the electric field is concentrated in the front of the nanoparticle. This situation well matches the radiation pattern in Fig. 4f, which shows a significant forward scattering amplification. Thereby, our analysis proves the connection between the multipole excitations, the far-field scattering, and the electric field concentration inside the particle for the different surrounding media. In addition, the broadening of the multipole moments especially the TED is of an importance for sensing applications. The reason for that is the weakening of the field inside the particle leads the multipole moments to be highly sensitive and endorse red shift when the surrounding medium refractive index change.

In Fig. 6a and b, we present the scattering cross-sections (Eq. 2) for the three cases of  $n = 1$ ,  $n = 1.6$  and  $n = 2$  along with the asymmetry parameter (Eq. 4). As expected, the multipole broadening afore-explained in Fig. 3 causes the synchronous overlapping of the multipoles of different orders and leads the asymmetry parameter to be dramatically broadened and enhanced as the surrounding medium refractive index increase. To clarify this point, in Fig. 6c we show the 2D radiation patterns for 6 different wavelengths over the spectrum for  $n = 2$  and a strong asymmetry remains for all spectral points. Thereby, the forward scattering amplification in the broad range is the

direct consequence of the high refractive index of the surrounding medium; the similar nanoantenna does not show such properties in case of  $n = 1$ .<sup>3</sup> Importantly, we note that the scattering efficiency for the cubical particle also enhanced over almost the whole optical range. This result can be widely implemented to develop nanoantennas and other optical devices for applications in non-air media like liquids and dielectric materials.

## **Conclusion**

To conclude, we studied the evolution of the multipole moments up to the third order for cubical nanoparticles embedded in different media and excited by a linearly polarized plane wave. We found that the electric multipole moments (TED, EQ) experience stronger redshift compared to the magnetic multipole moments (MD, MQ) as the index of medium increases. In addition, the separate scattering cross-section peaks transform to smoother merged peaks as the index of medium increases. However, the separate MQ and EQ resonances no longer exist for high-index surroundings. It is worth noting that the overall scattering cross-section of the silicon cube increases as  $n$  rises. To summarize, in this study, we show that the multipole decomposition method can be successfully applied for non-air surrounding media. For a better understanding of the medium influence, we considered 1) the far-field scattering patterns and 2) the electric field distributions inside the particles. Therefore, we discover that for a high-index surrounding media, the broadband forward scattering effect appears, while the backward scattering is simultaneously suppressed. For the same media, the electric field concentrates in the front part of the nanoscatteer; this effect correlates with the forward scattering amplification in the far-field. Outcomes of this research are essential for tuning the scattering direction just by changing the medium in which a nanoantenna is embedded. Based on that, variety of novel devices can be designed from sensing, health-care, monitoring to optical filters.

## **Acknowledgement**

This work has been supported by the Israeli Ministry of Trade and Labor-Kamin Program, Grant. No. 62045. A.S.S acknowledges the support of the Russian Fund for Basic Research within the projects 18-02-00414, 18-52-00005 and the support of the Ministry of Education and Science of the Russian Federation (GOSZADANIE Grant No. 3.4982.2017/6.7). The development of analytical approach and the calculations of multipole moments have been partially supported by the Russian Science Foundation Grant No. 16-12-10287. Support has been provided by the Government of the Russian Federation (Grant No. 08-08). The research described was performed by Pavel Terekhov as a part of the joint Ph.D. program between the BGU and ITMO.

## References

- (1) Karabchevsky, A.; Mosayyebi, A.; Kavokin, A. V. Tuning the Chemiluminescence of a Luminol Flow Using Plasmonic Nanoparticles. *Light Sci. Appl.* **2016**, *5* (11), e16164.
- (2) Kuznetsov, A. I.; Miroshnichenko, A. E.; Brongersma, M. L.; Kivshar, Y. S.; Lukyanchuk, B. Optically Resonant Dielectric Nanostructures. *Science* (80-. ). **2016**, *354* (6314), aag2472-aag2472.
- (3) Terekhov, P. D.; Baryshnikova, K. V; Artemyev, Y. A.; Karabchevsky, A.; Shalin, A. S.; Evlyukhin, A. B. Multipolar Response of Nonspherical Silicon Nanoparticles in the Visible and Near-Infrared Spectral Ranges. *Phys. Rev. B* **2017**, *96* (3), 35443.
- (4) Evlyukhin, A. B.; Reinhardt, C.; Seidel, A.; Lukyanchuk, B. S.; Chichkov, B. N. Optical Response Features of Si-Nanoparticle Arrays. *Phys. Rev. B* **2010**, *82* (4), 45404.
- (5) Kuznetsov, A. I.; Miroshnichenko, A. E.; Fu, Y. H.; Zhang, J.; Luk'yanchuk, B. Magnetic Light. *Sci. Rep.* **2012**, *2*, 492.
- (6) Evlyukhin, A. B.; Novikov, S. M.; Zywiets, U.; Eriksen, R. L.; Reinhardt, C.; Bozhevolnyi, S. I.; Chichkov, B. N. Demonstration of Magnetic Dipole Resonances of Dielectric Nanospheres in the Visible Region. *Nano Lett.* **2012**, *12* (7), 3749–3755.
- (7) Jahani, S.; Jacob, Z. All-Dielectric Metamaterials. *Nat. Nanotechnol.* **2016**, *11*, 23.
- (8) Ospanova, A. K.; Karabchevsky, A.; Basharin, A. A. Metamaterial Engineered Transparency Due to the Nullifying of Multipole Moments. *Opt. Lett.* **2018**, *43* (3), 503–506.
- (9) Basharin, A. A.; Kafesaki, M.; Economou, E. N.; Soukoulis, C. M.; Fedotov, V. A.; Savinov, V.; Zheludev, N. I. Dielectric Metamaterials with Toroidal Dipolar Response. *Phys. Rev. X* **2015**, *5*

(1), 11036.

- (10) Evlyukhin, A. B.; Reinhardt, C.; Chichkov, B. N. Multipole Light Scattering by Nonspherical Nanoparticles in the Discrete Dipole Approximation. *Phys. Rev. B* **2011**, *84* (23), 235429.
- (11) Bohren, C. F.; Huffman, D. R. *Absorption and Scattering of Light by Small Particles*; John Wiley & Sons, 2008.
- (12) Stockman, M. I. Nanoplasmonics: Past, Present, and Glimpse into Future. *Opt. Express* **2011**, *19* (22), 22029–22106.
- (13) Galutin, Y.; Falek, E.; Karabchevsky, A. Invisibility Cloaking Scheme by Evanescent Fields Distortion on Composite Plasmonic Waveguides with Si Nano-Spacer. *Sci. Rep.* **2017**, *7* (1), 12076.
- (14) Terekhov, P. D.; Baryshnikova, K. V.; Shalin, A. S.; Karabchevsky, A.; Evlyukhin, A. B. Resonant Forward Scattering of Light by High-Refractive-Index Dielectric Nanoparticles with Toroidal Dipole Contribution. *Opt. Lett.* **2017**, *42* (4), 835–838.
- (15) Jackson, J. D.; Fox, R. F. BOOK REVIEWS-Classical Electrodynamics. *Am. J. Phys.* **1999**, *67* (9), 841.
- (16) Krasnok, A. E.; Miroshnichenko, A. E.; Belov, P. A.; Kivshar, Y. S. All-Dielectric Optical Nanoantennas. *Opt. Express* **2012**, *20* (18), 20599–20604.
- (17) Rolly, B.; Stout, B.; Bonod, N. Boosting the Directivity of Optical Antennas with Magnetic and Electric Dipolar Resonant Particles. *Opt. Express* **2012**, *20* (18), 20376–20386.
- (18) Markovich, D.; Baryshnikova, K.; Shalin, A.; Samusev, A.; Krasnok, A.; Belov, P.; Ginzburg, P. Enhancement of Artificial Magnetism via Resonant Bianisotropy. *Sci. Rep.* **2016**, *6*, 22546.
- (19) Baryshnikova, K. V.; Novitsky, A.; Evlyukhin, A. B.; Shalin, A. S. Magnetic Field Concentration with Coaxial Silicon Nanocylinders in the Optical Spectral Range.
- (20) Kozlov, V.; Filonov, D.; Shalin, A. S.; Steinberg, B. Z.; Ginzburg, P. Asymmetric Backscattering from the Hybrid Magneto-Electric Meta Particle. *Appl. Phys. Lett.* **2016**, *109* (20), 203503.
- (21) Katiyi, A.; Karabchevsky, A. Figure of Merit of All-Dielectric Waveguide Structures for Absorption Overtone Spectroscopy. *J. Light. Technol.* **2017**, *35* (14), 2902–2908.
- (22) Bontempi, N.; Chong, K. E.; Orton, H. W.; Staude, I.; Choi, D.-Y.; Alessandri, I.; Kivshar, Y. S.; Neshev, D. N. Highly Sensitive Biosensors Based on All-Dielectric Nanoresonators. *Nanoscale* **2017**, *9* (15), 4972–4980.
- (23) Yavas, O.; Svedendahl, M.; Dobosz, P.; Sanz, V.; Quidant, R. On-a-Chip Biosensing Based on All-Dielectric Nanoresonators. *Nano Lett.* **2017**, *17* (7), 4421–4426.
- (24) Spinelli, P.; Verschuuren, M. A.; Polman, A. Broadband Omnidirectional Antireflection Coating

Based on Subwavelength Surface Mie Resonators. *Nat. Commun.* **2012**, *3*, 692.

- (25) Decker, M.; Staude, I.; Falkner, M.; Dominguez, J.; Neshev, D. N.; Brener, I.; Pertsch, T.; Kivshar, Y. S. High-Efficiency Dielectric Huygens' Surfaces. *Adv. Opt. Mater.* **2015**, *3* (6), 813–820.
- (26) Sayanskiy, A.; Danaeifar, M.; Kapitanova, P.; Miroshnichenko, A. E. All-Dielectric Metalattice with Enhanced Toroidal Dipole Response. *Adv. Opt. Mater.* **2018**, 1800302.
- (27) Fleury, R.; Monticone, F.; Alù, A. Invisibility and Cloaking: Origins, Present, and Future Perspectives. *Phys. Rev. Appl.* **2015**, *4* (3), 37001.
- (28) Zhao, Q.; Geng, H.; Wang, Y.; Gao, Y.; Huang, J.; Wang, Y.; Zhang, J.; Wang, S. Hyaluronic Acid Oligosaccharide Modified Redox-Responsive Mesoporous Silica Nanoparticles for Targeted Drug Delivery. *ACS Appl. Mater. Interfaces* **2014**, *6* (22), 20290–20299.
- (29) Hughes, G. A. Nanostructure-Mediated Drug Delivery. In *Nanomedicine in Cancer*; Pan Stanford, 2017; pp 47–72.
- (30) Blanco, E.; Shen, H.; Ferrari, M. Principles of Nanoparticle Design for Overcoming Biological Barriers to Drug Delivery. *Nat. Biotechnol.* **2015**, *33* (9), 941.
- (31) Salomatina, E. V.; Jiang, B.; Novak, J.; Yaroslavsky, A. N. Optical Properties of Normal and Cancerous Human Skin in the Visible and Near-Infrared Spectral Range. *J. Biomed. Opt.* **2006**, *11* (6), 64026.
- (32) Evlyukhin, A. B.; Fischer, T.; Reinhardt, C.; Chichkov, B. N. Optical Theorem and Multipole Scattering of Light by Arbitrary Shaped Nanoparticles. *Phys. Rev. B* **2016**, *94* (20), 205434.
- (33) Alaei, R.; Rockstuhl, C.; Fernandez-Corbaton, I. An Electromagnetic Multipole Expansion beyond the Long-Wavelength Approximation. *Opt. Commun.* **2018**, 407.
- (34) Terekhov, P. D.; Baryshnikova, K. V.; Evlyukhin, A. B.; Shalin, A. S. Destructive Interference between Electric and Toroidal Dipole Moments in TiO<sub>2</sub> Cylinders and Frustums with Coaxial Voids. In *Journal of Physics: Conference Series*; 2017; Vol. 929, p 12065.
- (35) Palik, E. D. *Handbook of Optical Constants of Solids*; Academic press, 1998; Vol. 3.
- (36) Pepper, D. W.; Heinrich, J. C. *The Finite Element Method: Basic Concepts and Applications with MATLAB, MAPLE, and COMSOL*; CRC Press, 2017.

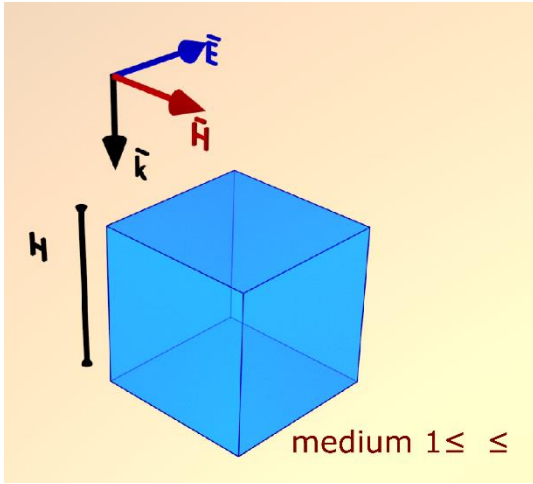


Figure 1: The schematics of the single particle suspended in a medium.

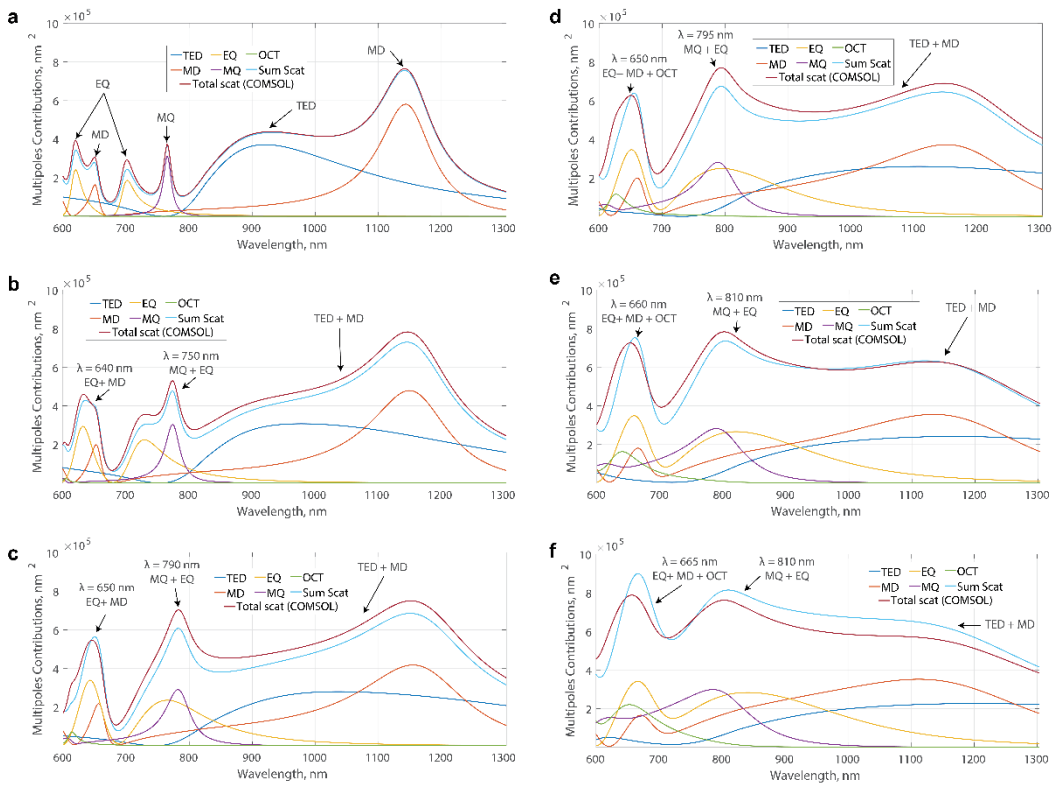


Figure 2: The multipole contributions to the scattering cross-section and the total scattering cross-sections of the silicon nanocube embedded in different media. The refractive indexes of surrounding media are (a)  $n = 1$  (b)  $n = 1.2$  (c)  $n = 1.4$  (d)  $n = 1.6$  (e)  $n = 1.8$  (f)  $n = 2$ . Sum Scat states for the scattering cross-section as the sum of the multipole contributions; Total scat (COMSOL) states for directly calculated scattering cross-section.

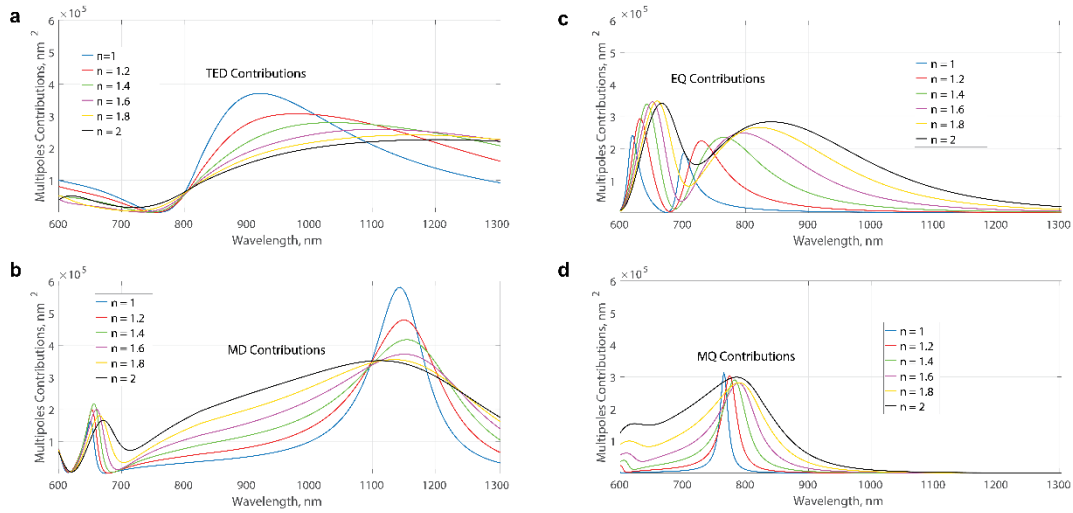


Figure 3: The multipole evolution of (a) the TED moment (b) the MD moment (c) the EQ moment (d) the MQ moment contribution to the scattering cross-section as the refractive index of surrounding medium rises.

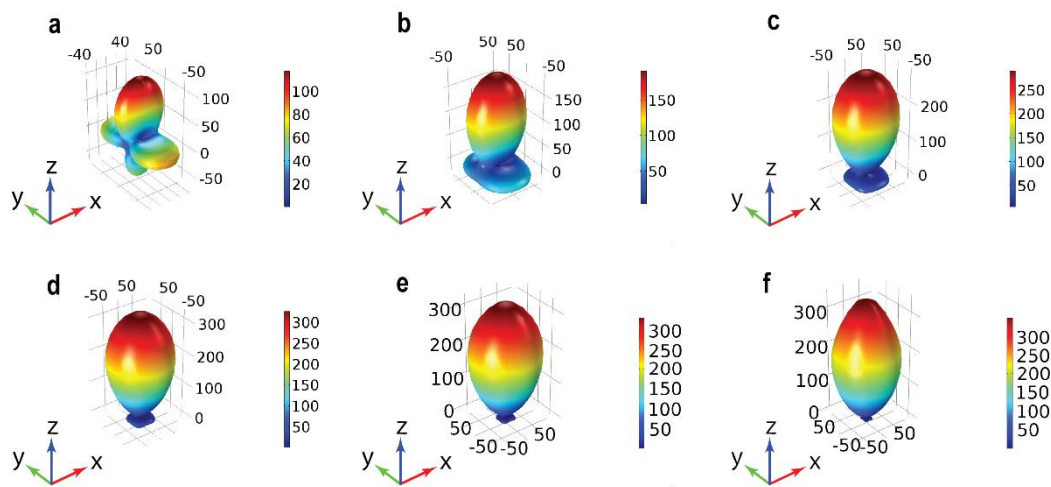


Figure 4: The radiation patterns for (a)  $n = 1, \lambda = 765 \text{ nm}$  (b)  $n = 1.2, \lambda = 775 \text{ nm}$  (c)  $n = 1.4, \lambda = 783 \text{ nm}$  (d)  $n = 1.6, \lambda = 789 \text{ nm}$  (e)  $n = 1.8, \lambda = 789 \text{ nm}$  (f)  $n = 2, \lambda = 789 \text{ nm}$ .

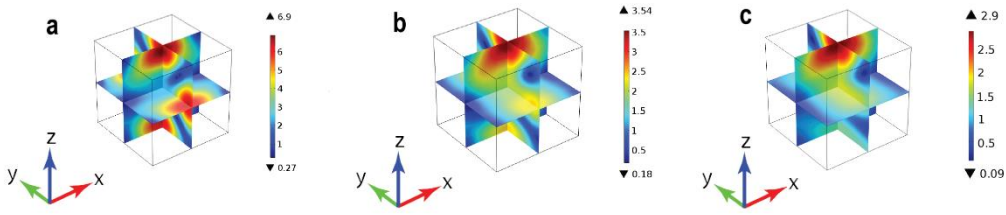


Figure 5: The electric field distribution inside the nanocube for (a)  $n = 1, \lambda = 765 \text{ nm}$  (b)  $n = 1.6, \lambda = 789 \text{ nm}$  (c)  $n = 2, \lambda = 789 \text{ nm}$ .

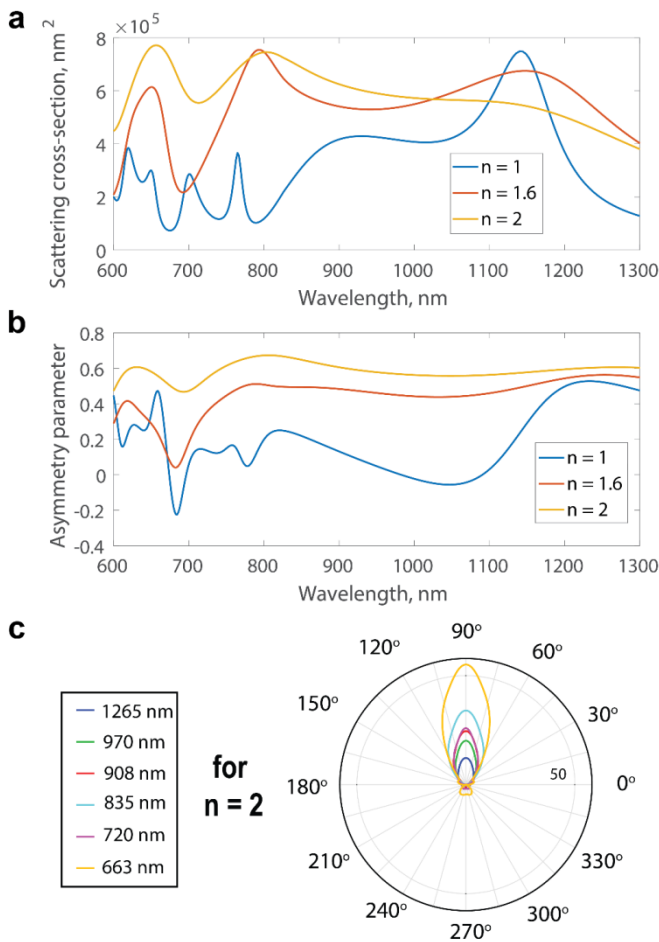


Figure 6: The scattering cross-section (a) and the asymmetry parameter (b) for  $250 \text{ nm}$  silicon cube embedded in a medium with  $n = 1, 1.6, 2$ . (c) The 2D radiation patterns in the medium with  $n = 2$  for various wavelengths  $\lambda$  as indicated in the legend. The radiation patterns are presented in the plane of the electric field polarization of the incident wave.